Molecular Pharmacology Fast Forward. Published on December 8, 2004 as doi:10.1124/mol.104.008888
This article has not been copyedited and formatted. The final version may differ from this version.

Title:

The aryl hydrocarbon receptor is required for developmental closure of the *ductus venosus* in the neonatal mouse

Authors:

Garet P. Lahvis, Robert W. Pyzalski, Edward Glover, Henry C. Pitot, Matthew K. McElwee, and Christopher A. Bradfield

Affiliations:

Department of Surgery[GPL, MKM], Department of Radiology[RWP] and McArdle Laboratory for Cancer Research[EG, HCP,CAB], University of Wisconsin Medical School, Madison, WI

Molecular Pharmacology Fast Forward. Published on December 8, 2004 as DOI: 10.1124/mol.104.008888
This article has not been copyedited and formatted. The final version may differ from this version.

Running Title: *Ahr* and ductus venosus

Corresponding Author:
Christopher A. Bradfield
McArdle Laboratory for Cancer Research
1400 University Ave., Madison, WI 53706
Tel.: 608-262-2024
Fax: 608-262-2824
E-mail: bradfield@oncology.wisc.edu.

Manuscript Information:
Number of text pages: 18
Number of tables: 0
Number of figures: 7
Number of references: 32
Abstract: 225 words
Introduction: 474 words
Discussion: 1395 words

Abbreviations:

Ahr:	aryl hydrocarbon receptor
PAS:	Per-Arnt-Sim
IVC:	inferior vena cava
DV:	ductus venosus
NBF:	neutral buffered formalin
PV:	portal vein
UV:	umbilical vein
H&E:	hemotoxylin and eosin stain
CT:	computerized tomography
MR:	magnetic resonance
VEGF:	vascular endothelial growth factor
DA:	ductus arteriosus
ha:	hepatic artery
bd:	bile duct
d:	diaphragm

Molecular Pharmacology Fast Forward. Published on December 8, 2004 as DOI: 10.1124/mol.104.008888
This article has not been copyedited and formatted. The final version may differ from this version.

ABSTRACT

A developmental role for the *Ahr* locus has been indicated by the observation that mice harboring a null allele display a porto-caval vascular shunt throughout life. To define the ontogeny and determine the identity of this shunt, we developed a visualization approach where three-dimensional (3D) images of the developing liver vasculature are generated from serial sections. Applying this 3D visualization approach at multiple developmental times allowed us to demonstrate that the porto-caval shunt observed in *Ahr* null mice is the remnant of an embryonic structure and is not acquired after birth. We observed that the shunt is found in late stage wild-type embryos, but closes during the first 48 hours of postnatal life. In contrast, the same structure fails to close in *Ahr* null mice and remains open throughout adulthood. The ontogeny of this shunt, along with its 3D position, allowed us to conclude that this shunt is a patent developmental structure known as the *ductus venosus* (DV). Upon searching for a physiological cause of the patent DV, we observed that during the first 48 hours, most major hepatic veins, such as the portal and umbilical veins, normally decrease in diameter, but do not change in *Ahr* null mice. This observation suggests that failure of the DV to close may be the consequence of increased pressure or a failure in vasoconstriction in the developing liver.

Molecular Pharmacology Fast Forward. Published on December 8, 2004 as DOI: 10.1124/mol.104.008888
This article has not been copyedited and formatted. The final version may differ from this version.

INTRODUCTION

The *Ahr* locus encodes the aryl hydrocarbon receptor (AHR), a basic-helix-loop helix PAS protein that is best known for its role in mediating biological responses to halogenated-dioxins and related toxic and carcinogenic environmental chemicals (Mimura and Fujii-Kuriyama, 2003). Recently, we have reported that this protein also plays an important role in vascular biology (Lahvis et al., 2000). Although *Ahr* null mice are viable, the liver size in these animals is approximately 30% smaller than wild-type controls. This hepatic phenotype is fully penetrant and is found in both adult male and female mice. Morphometric analysis indicates that the smaller liver is partially the result of decreased hepatocyte size (Lahvis et al., 2000). Our investigations into the cause of the smaller liver led to the discovery that adult *Ahr* null animals suffer from porto-caval shunting of blood within the liver parenchyma. Using adult mice, studies with micro-spheres indicate that more than half of the portal blood that flows to the liver bypasses the liver sinusoids in *Ahr* nulls (Lahvis et al., 2000). Latex-corrosion casts and time-lapse angiography in adult mice demonstrate that this bypass results from a single direct shunt between the portal vein (PV) and the inferior vena cava (IVC) (Lahvis et al., 2000).

We have been interested in the identity of the porto-caval shunt observed in adult *Ahr* null mice, as well as its physiological cause. The purpose of this study was to formally examine whether the shunt was congenital or acquired. As the result of our previous work, we postulated that this shunt might be a congenital phenomenon, the result of a patent fetal vascular structure known as the *ductus venosus* (DV)(Lahvis et al., 2000). The DV shunts umbilical blood through the liver to the inferior vena cava (IVC). Given that all of our prior analysis has been performed using adult animals, it is equally possible that this shunt was acquired as the result of some aberrant

liver physiology/pathology, for example, through the formation of collateral blood vessels related to portal hypertension (Datta et al., 1975; Sugiura et al., 1992).

In order to distinguish between possible congenital or acquired causes of this porto-caval shunt, we set out to understand the precise 3-dimensional (3D) position of this structure and how it changes over developmental time. To accomplish this objective, we evaluated the ontogeny of this shunt in normal and *Ahr* null mice by reconstructing 3D volumes of the liver vasculature at multiple prenatal and postnatal developmental times. Using this approach, we confirmed that the position and ontogeny of the porto-caval shunt in *Ahr* null mice is consistent with its identity as a patent DV and that this structure is not the result of a shunt that is acquired later in life. Moreover, we provide preliminary evidence that the patent DV may be the result of reduced vascular tone in the developing *Ahr* null liver.

Molecular Pharmacology Fast Forward. Published on December 8, 2004 as DOI: 10.1124/mol.104.008888
This article has not been copyedited and formatted. The final version may differ from this version.

MATERIALS AND METHODS

Mice

The *Ahr* null mouse colony (designated *Ahr* $^{-/-}$) used in these studies were congenic to the C57BL/6J (B6) background. This colony was generated by 20 backcrosses to the B6 strain (N20) with continual selection for the *Ahr* $^{-}$ allele. The *Ahr* $^{-/-}$ (null) and *Ahr* $^{+/+}$ (wild-type) controls were derived from intercrosses of *Ahr* $^{+/-}$ heterozygotes. All animals received humane care according to the criteria outlined in the "Guide for the Care and Use of Laboratory Animals" (National Research Council, Washington, 1996).

Caesarian-derivation

To establish the exact time of birth, mice were delivered by caesarian-derivation at E18.5. Briefly, the abdomen was incised, the uterus was removed, and fetuses were isolated from the visceral yolk sac and amnion. Pups were palpated with sterile cotton-tipped swabs to facilitate breathing. For fostering, pups were mixed with pups of a foster dam and when possible, with maternal urine. Pups of the foster dam were then removed and the foster dam was returned to the cage with the caesarian-derived animals.

Liver isolation and fixation

At specific times following caesarian-delivery, liver, lung, kidneys, stomach and intestines were quickly excised from euthanized newborn mice as a single unit. These organs were then dipped in 10 % (v/v) neutral buffered formalin (NBF) and suspended by the lungs to achieve a mild fixation of the liver lobes that reflected their natural position within the abdomen. Organs were then placed in 10% NBF and maintained at 4^{o}C overnight. After fixation, organs were rinsed and

Molecular Pharmacology Fast Forward. Published on December 8, 2004 as DOI: 10.1124/mol.104.008888
This article has not been copyedited and formatted. The final version may differ from this version.

stored in chilled ethanol: H_2O (70:30). Fixed livers were then dissected from the lungs and inferior regions of the small intestines. Care was taken to maintain the umbilical vein, supra-hepatic IVC, and portion of the diaphragm proximal to the IVC. Portions of the intestine and kidney were dissected to help in the identification of the infra-hepatic PV and IVC, respectively. Stomach contents were removed to minimize effects of stomach acids on H&E staining. Livers were embedded with the diaphragm and supra-hepatic IVC placed proximal to the bottom of the wax boat. Transverse serial sectioning began at the diaphragm and proceeded through to the kidneys. Serial liver sections of five microns thickness were obtained and digitally photographed, producing either 1090 x 1300 pixel images, using a Zeiss Axiocam on a Zeiss Axioplan 2 microscope, or 240 x 460 pixel images, using an Olympus OLY-750 CCD camera and a PC with a frame grabber card through a Navitar zoom 7000 lens.

Three-dimensional Reconstruction

Three-dimensional reconstruction requires the alignment and stacking of digital photographs of serial sections. Alignment is necessary for reconstruction from histological sections, since they are placed by hand on glass slides in a water bath. As a result, the orientation of each section relative to the glass slide is variable and photographs of each slide provide a range of orientations. Consequently, image-processing software was used to help align serial sections. This image registration procedure was performed on consecutive pairs of images throughout each stack (e.g., section 1 and 2, then 2 and 3 etc). The overlying section was first adjusted so that its center approximately overlapped that of the previous section. We then rotated the overlying image to re-establish the continuity of the majority of points from section to section. When all of the sections were aligned with one another, they were then combined into one 3D

image file per sample. The software that was used to align sections and stack them into a 3D image file was written in our lab, using VolPack (Lacroute and Levoy, 1994), and the XIL and XView libraries. The processing was done on a Sun Ultra 1 workstation running the Solaris operating system.

Projection images and movies of the 3D reconstructions were produced using Voxx, a volume rendering program which permits examination and manipulation of a stack of aligned 2D images in near real-time on a PC (Clendenon et al., 2002). Nonlinear intensity transformations and intensity-to-color mappings were used to improve the visibility of the vessels (Clendenon et al., 2002). Scale factors for the 3D images were computed using images of a stage micrometer slide and the thickness of the tissue sections. Examples of 3D images generated with Voxx are provided in Figures 2 and 4. To improve our ability to see of the vessels within the liver, the axis perpendicular to the plane of section was increased 3-fold relative to X and Y dimensions.

Fluorescence Imaging

To characterize the vascular structures of the neonatal brain, we stained the luminal surface of the vessels with a fluorescent-labeled lectin derived from the tomato *L. esculentum* (McDonald et al., 1999) (Vector Laboratories, Burlingame, CA). The intra-vascular space of a neonatal mouse was accessed by insertion of a pulled glass pipette (outer diameter of approximately 50 um) into the aortic arch. We used a micromanipulator to direct the pipette tip into the vessel and tie the vessel to the tip with a 10-0 suture. The descending aorta was occluded and the right atrium was incised. The neonatal brain was stained and fixed during the perfusion. Thick

sections (75 um) are obtained with a vibrating microtome and images were collected by fluorescence microscopy.

Vessel Diameters

The diameters of the IVC, PV, and umbilical vein (UV) were determined at their sites of entry to the liver. Measurements were typically taken from at least three individuals at each time-point. Three measurements of vessel diameter were collected from section photographs at 15 micron intervals from the site were the vessel was encapsulated by the liver. Measurements of DV diameter were made at the intra-hepatic site where the DV was narrowest. Measurements were calibrated with a stage micrometer and analysis of variance was used for statistical comparison of vessel diameters (Sokal and Rohlf, 1995).

Molecular Pharmacology Fast Forward. Published on December 8, 2004 as DOI: 10.1124/mol.104.008888
This article has not been copyedited and formatted. The final version may differ from this version.

RESULTS

Identification of major hepatic veins

Identification of the DV in newborn mice was accomplished by its unique vascular connections. The DV is the only fetal vessel that shunts blood to the IVC and to the PV, thereby providing retrograde perfusion of the liver (see Fig. 1A). To locate the DV, we first identified the fetal UV, PV and the IVC as reference vascular structures within the liver. Each of these vessels was identified by virtue of their distinct anatomical characteristics and position of entry into the developing liver. The PV is a relatively small vessel that drains the esophagus, stomach, intestines, spleen, pancreas, and gall bladder. The PV enters the liver via a central site, adjacent to the hepatic artery, between the right and left lobes. A transverse section through its liver entry point is shown (Fig. 1B). The UV enters the median lobe of the liver, adjacent to the gall bladder and associated bile duct, and typically narrows as it enters the liver (Fig. 1C). The infra-hepatic IVC is associated with renal veins inferior to the liver and enters to the liver via the distal region of the right lobe (Fig. 1D). The supra-hepatic IVC leaves the liver and traverses the diaphragm (Fig. 1E).

Vascular anatomy of neonatal liver can be described by 3D reconstruction

To visualize the hepatic blood vessels by 3D reconstruction, we began by highlighting all of the blood vessels of greater than approximately 25 microns in diameter in each section. In every section through the liver, standard thresholding tools were employed to delineate the vascular lumen from surrounding parenchyma (e.g., “clear” vs. “stained”). Vessel lumens were highlighted in black and photographs were then converted from RGB to grayscale format. In the

final reconstructions used to generate figures, the grayscale was inverted so that vessels are visible as white structures in gray parenchyma on a black background.

Figure 2 provides an example of the flexibility, quality and resolution of the 3D images generated by this approach. These 2D images represent "screen shots" from different turns of the 3D images generated by reconstruction of the major hepatic blood vessels of a wild-type mouse at 24 hours of age. By modifying threshold values from the reconstruction, we are able to see either the surface of the tissue, in this case the abdominal cavity and its associated organs (Fig. 2A) or a similarly positioned internal vascular pattern which highlights only the hepatic vasculature (Fig. 2B). Surface imaging shows the liver (L) from different angles, allowing us to see the associated diaphragm (D), spleen (S), kidneys (K), and intestine (I) (Fig. 2A). Surface imaging also allows us to see the renal veins (RV) at the inferior end of the reconstruction and the supra-hepatic IVC as it leaves the diaphragm. When we change threshold settings for the volume, the surface image becomes a faint "ghost" and we can visualize the large hepatic vessels that have been highlighted (Fig. 2B). We can clearly identify the IVC, which runs from the kidneys through the liver, and the UV from several orientations. However, the PV and DV remain obscured by many vessel branches that proceed through the liver lobes.

To identify the DV, we relied upon its distinct anatomy as the only vessel that connects the fetal PV, UV and IVC. All other hepatic vascular structures emanate from these larger vessels and then continue to branch, forming much finer structures that terminate in the distal regions of the liver. In order to facilitate viewing the DV, we removed any vasculature structure from the 3D image that terminated in a liver lobe. Using this technique, we were able to visualize only the

Molecular Pharmacology Fast Forward. Published on December 8, 2004 as DOI: 10.1124/mol.104.008888
This article has not been copyedited and formatted. The final version may differ from this version.

UV, PV and IVC (Fig. 3). The PV was identifiable as a smaller vessel running parallel with the IVC and meeting the UV in a region where the major branches of each lobe converge. We also obtained an unobstructed view of the DV (Fig. 3B), which meets with the IVC, in transverse planes that are anterior to the PV/UV junction. In combination, these techniques illustrated proof of concept that serial reconstruction of histological sections could be used to identify the DV in neonatal mice.

Failure of DV closure in *Ahr* null mice

To determine if the porto-caval shunt in *Ahr* null mice is a patent DV, we compared the ontogeny of this structure in wild-type and *Ahr*-null mice. To accomplish this we generated 3D reconstructions from both mouse strains at neonatal ages, ranging from newborn to 48 hours old. Since birth of a litter typically occurs over several hours, we performed Caesarian derivations of pregnant females at E18.5 to normalize the birth hour of newborn pups. Livers were collected, sectioned, stained, photographed, rendered and reconstructed from mice sacrificed at 1, 6, 12, 18, 24, and 48 hours after birth (as described above). The vascular structures of the reconstructions were then modified to emphasize only the PV, UV, IVC and DV (as described above). These 3D images clearly show the presence of the DV at birth and 6 hours of age in both wild-type (Figs 4A and B) and *Ahr* null (Figs. 4G and H) livers. In wild-type mice, the DV appears to have a more restricted diameter at 24 hours of age (Fig. 4E) and the vessel disappears completely by 48 hours of age (Fig. 4F). By contrast, the DV remains fully open through 48 hours of age in the null mice (Figs. 4G-L).

Molecular Pharmacology Fast Forward. Published on December 8, 2004 as DOI: 10.1124/mol.104.008888
This article has not been copyedited and formatted. The final version may differ from this version.

The 3D reconstructions illustrate a variety of shapes for the IVC, PV, and UV in these livers. These patterns reflect differences in the arrangement of the liver, kidneys, spleen and intestines during fixation. Some variability in vessel morphology in the 3D images reflects subtle changes in liver shape due to fixation. Despite efforts to control the spatial organization of the liver, some liver lobes spread out in fixative but not in others.

Cellular composition of the DV is similar in *Ahr* null and wild-type mice

Once evidence of a patent DV in *Ahr* null mice was generated, the individual H&E stained slides containing this structure were examined for histological evidence of pathology at this site. This analysis was performed in several mice at ages ranging from 6 hours to 48 hours of age. Measurements were typically taken from at least three individuals at each time-point. Although we were able to identify basophilic hematopoietic cells lining the DV of both normal and *Ahr* null mice, we were unable to find clear differences in the cellular composition of the DV between these two strains between birth and 24 hours of age (Fig.5).

Diameters of major intra-hepatic vessels do not contract after birth in *Ahr* null mice

The 3D reconstructions were valuable for identification of the DV and for illustration that the DV closes in wild-type, but not *Ahr* null mice. To compare vessel diameters in *Ahr* null mice and wild-type controls, we measured diameters in histological sections of age-matched livers at 6, 12, 24 and 48 hours of age. Analysis of this data indicates that the wild-type UV diameter decreased from 212 to 106 microns ($p= 0.003$) from 6 to 48 hours (Fig. 6, lower left panel). The PV diameter also decreased from 198 to 65 microns ($p=0.0001$) in wild-type mice during this time period (Fig. 6, upper left panel). Though not significant ($p=0.12$), there was trend towards

decreased diameter of the IVC in wild-type mice (170 to 101 microns) (Fig. 6, upper right panel).

In wild-type mice, the average lumen diameter of the DV decreased in size from 162 to 6 microns diameter between ages of 6 and 48 hours (Fig. 6, lower right panel). Decreased DV diameter in wild-type mice was significant by as early as 12 hours of age (162 to 62 microns, p=0.007). At 24 hours of age, we found resolution of only 1 DV among 4 wild-type mice. By 48 hours of age, DV resolution was complete in 80 percent of the wild-type mice (4/5) examined. By contrast, the DV was fully patent in all *Ahr* null mice at 24 hours (0/4 resolved) and at 48 hours of age (0/4 resolved). Vessels in null livers over the first 48 hours did not change in diameter, resulting in significantly greater diameters of null versus wild-type vessels. At 48 hours of age, vessel diameters of the *Ahr* null PV (p = 0.0064), UV (P = 0.0022), and DV (p = 0.0009) were significantly greater than those of the wild-type controls. IVC diameter was not significantly greater in *Ahr* null livers at 48 hours (p = 0. 1011).

Vessel diameters in the brain are similar between *Ahr* null and wild-type mice

Given that hepatic vessel diameter was increased in the *Ahr* null animals, we wondered if this phenotype was a generalized vascular phenomenon. Therefore, we set out to examine non-hepatic vessel diameters in the *Ahr* null mouse at 48 hours of age. To this end, we evaluated the morphology of capillaries and small vessels in identical regions of the mouse brain at 48 hours of age. Blood vessels of *Ahr* heterozygous (Fig. 7A) and homozygous (Fig. 7B) null mice of 48 hours of age were visualized by fluorescence microscopy. Capillary diameters were found to be equivalent in *Ahr* null animals and their heterozygous controls, with average diameters of 5.7

(SD=0.26) and 5.5 microns (SD=0.51), respectively. Similarly, small vessels in the *Ahr* null mouse (90 microns, SD=14.4) were similar in diameter to vessels in the wild-type control (83 microns, SD=4.6).

Molecular Pharmacology Fast Forward. Published on December 8, 2004 as DOI: 10.1124/mol.104.008888
This article has not been copyedited and formatted. The final version may differ from this version.

DISCUSSION

Background

The purpose of this study was to examine the two most likely underlying causes of porto-caval shunting in *Ahr* null mice. We attempted to determine whether the shunt observed in adult *Ahr* null mice represents the persistence of the fetal structure known as the DV or if it is the result of a distinct collateral blood vessel that arose from an independent process. To make this distinction, we generated 3D images of the developing vascular architecture from serial histological sections of the neonatal mouse liver and abdomen. Using this approach, we were able to reliably identify the PV, IVC UV and DV. We found that the DV normally closes within 48 hours after parturition in wild-type mice but remains patent in *Ahr* null animals. In previous reports, we postulated that this porto-caval shunt might be a patent DV, but this is the first formal evidence that this structure represents such a structure and that it defines a congenital aberration inherent to the *Ahr* null genotype. Our conclusion does not support conjecture that the shunt represents an acquired structure generated later in life. Taken in sum, these data provide compelling evidence that the AHR plays an important role in the normal development of the hepatic vascular architecture, with a hallmark effect of the null phenotype being failure of DV closure.

Advantages of 3D imaging by serial reconstruction

Three-dimensional reconstruction of the developing vascular architecture required extensive tissue sectioning and use of novel computer software. Yet, the 3D images provide considerable power and flexibility and hold the potential to yield a vast amount of information about vascular morphology and the relationship between blood vessel position and organ morphology. The

Molecular Pharmacology Fast Forward. Published on December 8, 2004 as DOI: 10.1124/mol.104.008888
This article has not been copyedited and formatted. The final version may differ from this version.

power of this approach is that it allows the image to be turned along any axis (X, Y or Z) for more careful examination of the relationships between different blood vessels and surrounding structures (Fig. 2). We can thereby identify and follow the PV, IVC and UV into the neonatal liver lobes. Such tracking was essential to formally and reproducibly define the DV. Upon examining livers from mice 6-48 hours after birth, we rapidly and conclusively identified the DV from adjacent branches of the major vessels and were able to characterize its anatomy and how it changed over time relative to other vascular and histological features.

Although considerable technical hurdles had to be overcome, we chose to employ the 3D reconstruction approach over more classical approaches of vascular imaging. Historically, vascular architecture has often been visualized in 3D by perfusion of plastic resins into tissues, followed by digestion of surrounding parenchyma to create a cast or physical model of the intra-vascular space (Kondo, 1998; Lahvis et al., 2000; Mironov et al., 1994; Navarro et al., 2003). The advantages of 3D reconstruction from serial sections over latex cast methods are multiple. First, unlike latex casts, the 3D images generated by reconstruction are digitized and thus are readily viewed, archived and shared between investigators. Second, unlike latex casts, the reconstruction approach is derived from histological sections, so we have the unique ability to model the architecture of a vascular structure, identify a region of interest, and re-examine the corresponding sections at high magnification. This capacity allows study of the cellular or molecular characteristics of the vascular feature of interest (e.g., Fig. 5). In latex casts, such material is removed. Finally, latex casts of complex vascular structures are often difficult to interpret in regions where vascular structures are dense or intersect. In the 3D reconstruction

Molecular Pharmacology Fast Forward. Published on December 8, 2004 as DOI: 10.1124/mol.104.008888
This article has not been copyedited and formatted. The final version may differ from this version.

approach, such regions can be examined after digital pruning of overlapping or intersecting structures that obscure a region of interest (e.g. Fig. 3).

We find that 3D reconstructions generated from histological sections provide advantages that cannot be obtained from non-invasive imaging modalities, such as micro-CT, PET scanning, or MRI imaging. Non-invasive modalities do not yet provide information regarding cell composition and gene expression at levels of resolution that are readily achieved with light microscopy (Huang et al., 1996; Kantor et al., 2000; Sharma et al., 2002). Importantly, 3D reconstructions also provide advantages for vascular imaging that cannot be obtained from confocal and multi-photon microscopy, which generate 3D images limited to a few hundred microns in section thickness (Phillips et al., 2001). To reconstruct vascular patterns that exist throughout an organ, even confocal and multi-photon microscopy would require 3D reconstruction from multiple sections, as performed here.

Mechanism of DV closure and patency

The mechanism of DV closure is likely to be distinct from that for closure of the ductus arteriosus (DA). Resolution of the DA involves a rapid "functional constriction" followed by "anatomic closure," which permanently removes the vessel (Smith, 1998). The DV is unlikely to undergo functional constriction because an elastin-mediated sphincter has not been identified within the DV of humans or dogs (Burton and White, 1999; Mavrides et al., 2002). Such a structure was also not observed here. The difference in the timing of closure is also different. In humans, functional constriction results in DA closure within three days of birth (Alenick et al., 1992), whereas in humans the DV requires over two weeks to resolve (Fugelseth et al., 1999).

Molecular Pharmacology Fast Forward. Published on December 8, 2004 as DOI: 10.1124/mol.104.008888
This article has not been copyedited and formatted. The final version may differ from this version.

Additional evidence that these structures close by different mechanisms is that the DA is resolved in adult *Ahr* null mice (Lahvis et al., 2000) but that the DV remains patent in this same mutant strain.

We were interested in the possibility that the mechanism for resolution of the DV resembles that of neonatal capillary beds. In mammals, many small neonatal vessels close within three weeks after birth, including arterio-venous shunts on the brain surface (Feher et al., 1996; Krolo and Hudetz, 1998; Wang et al., 1992), membrane capillaries and vitrial arteries of the eye (Ito and Yoshioka, 1999; Lang and Bishop, 1993; Mitchell et al., 1998), lung capillaries (Zeltner and Burri, 1987), and liver sinusoids (Kiserud, 2001; McCuskey et al., 1997). In the neonatal eye, resolution of capillaries of the papillary membrane is thought to be due to macrophage accumulation (Ito and Yoshioka, 1999; Lang and Bishop, 1993), resulting in reduced blood flow, localized ischemia, VEGF deprivation (Meeson et al., 1999) and endothelial cell apoptosis (Meeson et al., 1996; Meeson et al., 1999). Our data is inconsistent with macrophage accumulation as an essential step in DV closure, as histological analysis did reveal evidence of large numbers of macrophages adjacent to the DV in normal development.

We have previously noted vascular changes in other organs of the *Ahr* null mouse including a persistent hyaloid artery, expansion of limbal vessels of the eye, and altered vascular density of the kidney. Whether these vascular alterations are a direct result of the lack of AHR signaling, or whether they are a consequence of altered vascular flow due to the patent DV, cannot be determined from these studies. However, it is clear that the vascular changes resulting from an

Molecular Pharmacology Fast Forward. Published on December 8, 2004 as DOI: 10.1124/mol.104.008888
This article has not been copyedited and formatted. The final version may differ from this version.

Ahr null allele occur in a number of organ systems, yet do not appear to extend to every organ system.

The results that have arisen from this 3D image analysis through development have led us to speculate on a mechanism to explain the patent DV in *Ahr* null mice. In the regard, we observed that wild-type neonatal hepatic vessels constrict by approximately the second day after birth. Yet, this developmentally mediated constriction does not occur as robustly in *Ahr* null mice. Our data suggest that hepatic vessel constriction is attributable to some aspect of AHR signaling. In mice harboring the *Ahr* null allele, this receptor-mediated event is lost leading to increased vasodilation and inefficient DV closure.

Summary

Using 3D reconstructions from serial histological sections, we have been able to evaluate hepatic vascular development in the neonatal mouse. Our approach allowed us to evaluate DV closure within the context of whole organ vascular patterns, as well as view this biology within the context of neighboring cellular constituents. Our results demonstrate that the *Ahr* is necessary for resolution of the DV, a shunt that normally closes within two days after birth in mice. This aberration in early vascular development in *Ahr* null mice, rules out the alternative explanation that an acquired shunt emerged later in life. These data also lend support to the hypothesis that normal DV closure is related to a generalized decrease in the diameter of the major vessels of the liver post-partum. The inefficiency of this neonatal vasoconstriction may explain the failure of DV closure in *Ahr* null mice.

ACKNOWLEDGEMENTS

Three-dimensional images in figures 2,3 and 5 were generated by with Voxx by Jeffrey L. Clendenon at the Indiana Center for Biological Microscopy, Indiana University School of Medicine. We thank Jacqueline Walisser for assistance in manuscript preparation.

REFERENCES

Alenick, D. S., Holzman, I. R., and Ritter, S. B. (1992). The neonatal transitional circulation: a combined noninvasive assessment. Echocardiography *9*, 29-37.

Burton, C. A., and White, R. N. (1999). The angiographic anatomy of the portal venous system in the neonatal dog. Res Vet Sci *66*, 211-217.

Clendenon, J. L., Phillips, C. L., Sandoval, R. M., Fang, S., and Dunn, K. W. (2002). Voxx: a PC-based, near real-time volume rendering system for biological microscopy. Am J Physiol Cell Physiol *282*, C213-218.

Datta, D. V., Grover, S. L., Saini, V. K., Datta, B. N., Aikat, B. K., and Chhuttani, P. N. (1975). Portal hypertension in chronic leukaemia. Br J Haematol *31*, 279-285.

Feher, G., Schulte, M. L., Weigle, C. G., Kampine, J. P., and Hudetz, A. G. (1996). Postnatal remodeling of the leptomeningeal vascular network as assessed by intravital fluorescence video-microscopy in the rat. Brain Res Dev Brain Res *91*, 209-217.

Fugelseth, D., Kiserud, T., Liestol, K., Langslet, A., and Lindemann, R. (1999). Ductus venosus blood velocity in persistent pulmonary hypertension of the newborn. Archives of Disease in Childhood: Fetal & Neonatal Edition *81*, F35-39.

Huang, W., Plyka, I., Li, H., Eisenstein, E. M., Volkow, N. D., and Springer, C. S., Jr. (1996). Magnetic resonance imaging (MRI) detection of the murine brain response to light: temporal differentiation and negative functional MRI changes. Proc Natl Acad Sci USA *93*, 6037-6042.

Ito, M., and Yoshioka, M. (1999). Regression of the hyaloid vessels and pupillary membrane of the mouse. Anat Embryol *200*, 403-411.

Kantor, B., Ritman, E., Holmes, D., and Schwartz, R. (2000). Imaging angiogenesis with three-dimensional microscopic computed tomography. Curr Interv Cardiol Rep *2*, 204-212.

Kiserud, T. (2001). The ductus venosus. Semin Perinatol *25*, 11-20.

Kondo, S. (1998). Microinjection methods for visualization of the vascular architecture of the mouse embryo for light and scanning electron microscopy. J Electron Microsc *47*, 101-113.

Krolo, I., and Hudetz, A. G. (1998). Remodeling of the leptomeningeal microvascular plexus in neonatal rats. Adv Exp Med Biol *454*, 349-354.

Lacroute, P., and Levoy, M. (1994). Fast Volume Rendering Using a Shear-Warp Factorization of the Viewing Transformation. Paper presented at: SIGGRAPH '94 (Orlando, Florida).

Lahvis, G. P., Lindell, S. L., Thomas, R. S., McCuskey, R. S., Murphy, C., Glover, E., Bentz, M., Southard, J., and Bradfield, C. A. (2000). Portosystemic shunting and persistent fetal vascular structures in aryl hydrocarbon receptor-deficient mice. Proc Natl Acad Sci USA *97*, 10442-10447.

Lang, R. A., and Bishop, J. M. (1993). Macrophages are required for cell death and tissue remodeling in the developing mouse eye. Cell *74*, 453-462.

Mavrides, E., Moscoso, G., Carvalho, J. S., Campbell, S., and Thilaganathan, B. (2002). The human ductus venosus between 13 and 17 weeks of gestation: histological and morphometric studies. Ultrasound Obstet Gynecol *19*, 39-46.

McCuskey, R. S., Ekataksin, W., LeBouton, A. V., Nishida, J., Krasovich, M. A., McDonnell, D., Williams, C., and Koldovsky, O. (1997). Development of hepatic sinusoidal structure and function in suckling rats. In Cells of the Hepatic Sinusoid VI, E. Wisse, D. L. Knook, and C. Balabaud, eds. (Leiden, Kupffer Cell Foundation), pp. 67-70.

McDonald, D. M., Thurston, G., and Baluk, P. (1999). Endothelial gaps as sites for plasma leakage in inflammation. Microcirculation *6*, 7-22.

Meeson, A., Palmer, M., Calfon, M., and Lang, R. (1996). A relationship between apoptosis and flow during programmed capillary regression is revealed by vital analysis. Dev *122*, 3929-3938.

Meeson, A. P., Argilla, M., Ko, K., Witte, L., and Lang, R. A. (1999). VEGF deprivation-induced apoptosis is a component of programmed capillary regression. Dev Suppl *126*, 1407-1415.

Mimura, J., and Fujii-Kuriyama, Y. (2003). Functional role of AhR in the expression of toxic effects by TCDD. Biochim Biophys Acta *1619*, 263-268.

Mironov, V., Hritz, M. A., LaManna, J. C., Hudetz, A. G., and Harik, S. I. (1994). Architectural alterations in rat cerebral microvessels after hypobaric hypoxia. Brain Res *660*, 73-80.

Mitchell, C. A., Risau, W., and Drexler, H. C. (1998). Regression of vessels in the tunica vasculosa lentis is initiated by coordinated endothelial apoptosis: a role for vascular endothelial growth factor as a survival factor for endothelium. Dev Dyn *213*, 322-333.

National Research Council. Washington, D. (1996). Guide for the Care and Use of Laboratory Animals. (Washington, DC, National Academy Press).

Navarro, M., DeRuiter, M. C., Carretero, A., and Ruberte, J. (2003). Microvascular assembly and cell invasion in chick mesonephros grafted onto chorioallantoic membrane. J Anat *202*, 213-225.

Phillips, C. L., Arend, L. J., Filson, A. J., Kojetin, D. J., Clendenon, J. L., Fang, S., and Dunn, K. W. (2001). Three-dimensional imaging of embryonic mouse kidney by two-photon microscopy. Am J Pathol *158*, 49-55.

Sharma, V., Luker, G. D., and Piwnica-Worms, D. (2002). Molecular imaging of gene expression and protein function in vivo with PET and SPECT. J Magn Res Imaging *16*, 336-351.

Smith, G. C. (1998). The pharmacology of the ductus arteriosus. Pharmacol Rev *50*, 35-58.

Sokal, R. R., and Rohlf, F. J. (1995). Biometry: the principles and practice of statistics in biological research, 3rd ed (New York, W. H. Freeman and Co.).

Sugiura, N., Karasawa, E., Saotome, N., Miki, M., Matsutani, S., and Ohto, M. (1992). Portosystemic collateral shunts originating from the left portal veins in portal hypertension: demonstration by color Doppler flow imaging. J Clin Ultrasound *20*, 427-432.

Wang, D. B., Blocher, N. C., Spence, M. E., Rovainen, C. M., and Woolsey, T. A. (1992). Development and remodeling of cerebral blood vessels and their flow in postnatal mice observed with in vivo videomicroscopy. J Cereb Blood Flow Metab *12*, 935-946.

Zeltner, T. B., and Burri, P. H. (1987). The postnatal development and growth of the human lung. II. Morphology. Respir Physiol *67*, 269-282.

FOOTNOTES

a.) Financial Support

Financial support for this study was provided by the National Institutes of Health Grants P30-CA014520, P01-CA022484, F32-ES05887 and with partial funding from a University of Wisconsin Department of Surgery Research Grant.

b.) Person receiving reprints: none at this time

c.) Numbered footnotes: none

Molecular Pharmacology Fast Forward. Published on December 8, 2004 as DOI: 10.1124/mol.104.008888
This article has not been copyedited and formatted. The final version may differ from this version.

FIGURE LEGENDS

Fig. 1. The IVC, PV and UV can be identified at entry to the liver. A, a schematic representation of major hepatic vessels including the portal vein (PV), umbilical vein (UV), and inferior vena cava (IVC). The fetal liver (thin red line) and diaphragm (thick red line) are also represented. B, the PV drains the gut and enters the liver between all of the lobes in association with the hepatic artery (ha). C, the UV enters the liver through the median lobe adjacent to the bile duct (bd). D, the infra-hepatic IVC drains the renal veins and then enters the distal portion of the right posterior lobe. E, the IVC then traverses the right posterior lobe and the IVC exits through the diaphragm (d).

Fig. 2. 3D reconstructions identify the major vessels in a neonatal mouse liver in the context of liver morphology. Vascular patterns of the liver were reconstructed in three dimensions to highlight either organ morphology (A) or hepatic blood vessels (B) from several viewing perspectives. In panel A, we can see the liver lobes (L), which are obscured proximally by the diaphragm (D). We also see the spleen (S) and kidneys (K) inferior and posterior to the distal portions of the liver lobes. Intestines (I) are also visible. When organ surfaces are presented as "ghosts," the IVC, renal veins (RV), and umbilical vein (UV) become visible. In these reconstructions, the ductus venosus remains obscured by surrounding vessels.

Fig. 3. Vascular reconstructions can be pruned to identify the DV. A, when all vessels greater than approximately 25 microns in diameter are highlighted, the ductus venosus (DV) remains obscured by surrounding vessels. B, in order to isolate the DV, we highlighted only the

IVC, PV, and UV and the one vessel that connects them (DV). Panels A and B show vascular patterns in 3D reconstructions that are projected in the same orientation.

Fig. 4. Three dimensional reconstructions of the vascular network of wild-type and *Ahr* null mouse livers. 3D reconstructions of major vessels of both wild-type (A-F) and *Ahr* null (G-L) livers show resolution of the DV in wild-type, but not *Ahr* null mice over the first 48 hours of age. Reconstructions were generated for mice of 1 (A,G), 6 (B,H), 12 (C,I), 18 (D,J), 24 (E,K), and 48 (F,L) hours of age. In wild-type mice, the DV is completely resolved by 48 hours of age (F), whereas the DV remains fully patent in *Ahr* null animals (L).

Fig. 5. Cellular composition of the DV is similar for wild-type and *Ahr* null mice. Serial sections through the DV in wild-type (left) and *Ahr* null (right) livers were evaluated to determine if the histology of the DV was different in wild-type versus *Ahr* null mice. Evaluation of DV histology at 6, 12, and 24 hours of age show occasional areas of hematopoietic cells (hc), which appear more basophilic than the adjacent hepatocytes, in both wild-type and *Ahr* null mice, but we found no consistent differences between alleles.

Fig. 6. Major veins of *Ahr* null livers have increased diameters at 48 hours of age. Diameters of the IVC, PV, UV, and DV were measured at specific points within the liver for an average of 3.8 mice per group at 6,12, 24, and 48 hours of age. Values for individual mice are plotted for wild-type (gray) and *Ahr* null (black) mice for the PV, UV, IVC, and DV. * indicates statistical significance at $P < 0.01$.

Molecular Pharmacology Fast Forward. Published on December 8, 2004 as DOI: 10.1124/mol.104.008888
This article has not been copyedited and formatted. The final version may differ from this version.

Fig 7. Diameters of capillaries in brain are similar in *Ahr* heterozygous and homozygous null mice. Capillaries of *Ahr* heterozygous (A) and homozygous (B) null mice at 48 hours of age were visualized by fluorescence microscopy. Capillaries (c) were identified by their consistently small diameter and were found to be equivalent in null and control animals. To measure small vessel diameters (sv), we identified a group of vessels in a small region of the brain near the substantia nigra, and measured diameters for all of the vessels in this group.

Figure 1.

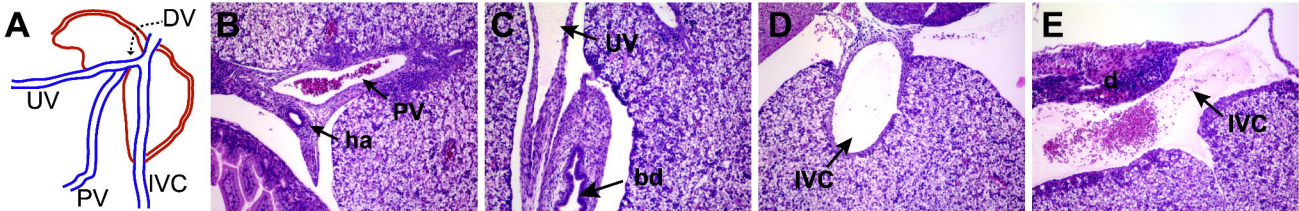

Figure 2.

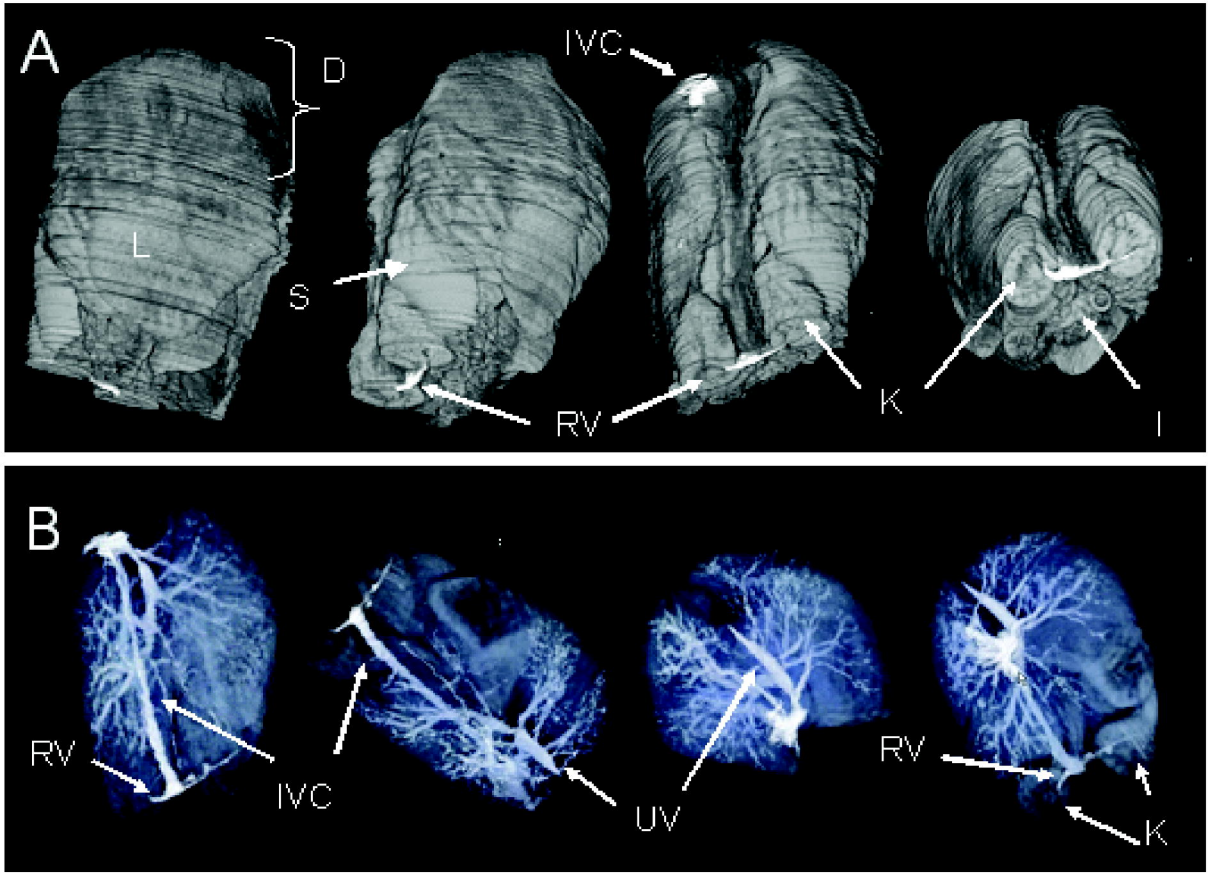

Figure 3.

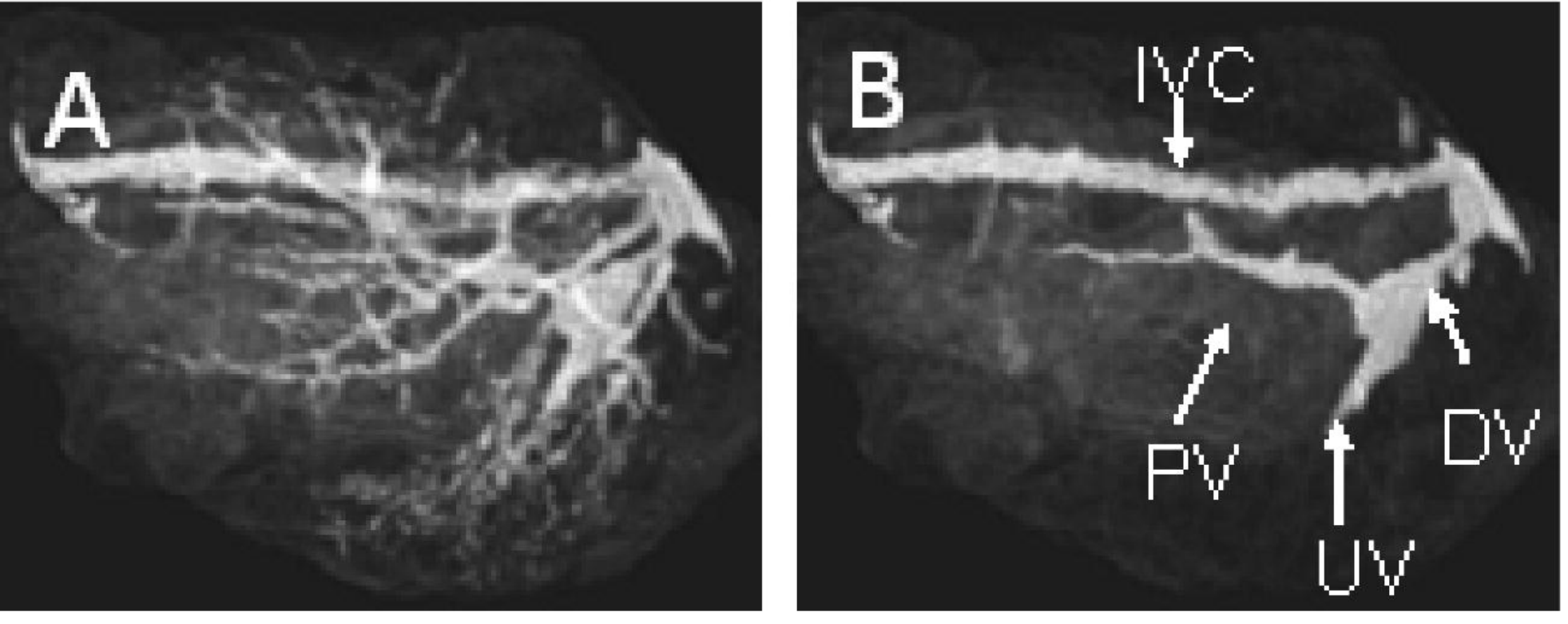

Figure 4.

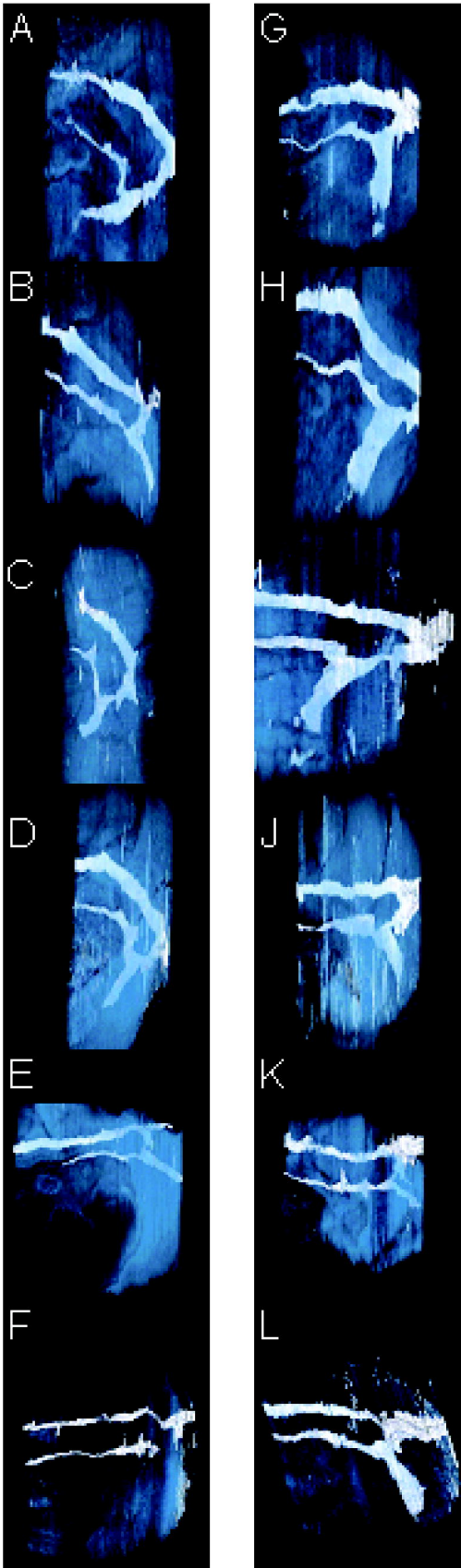

Figure 5.

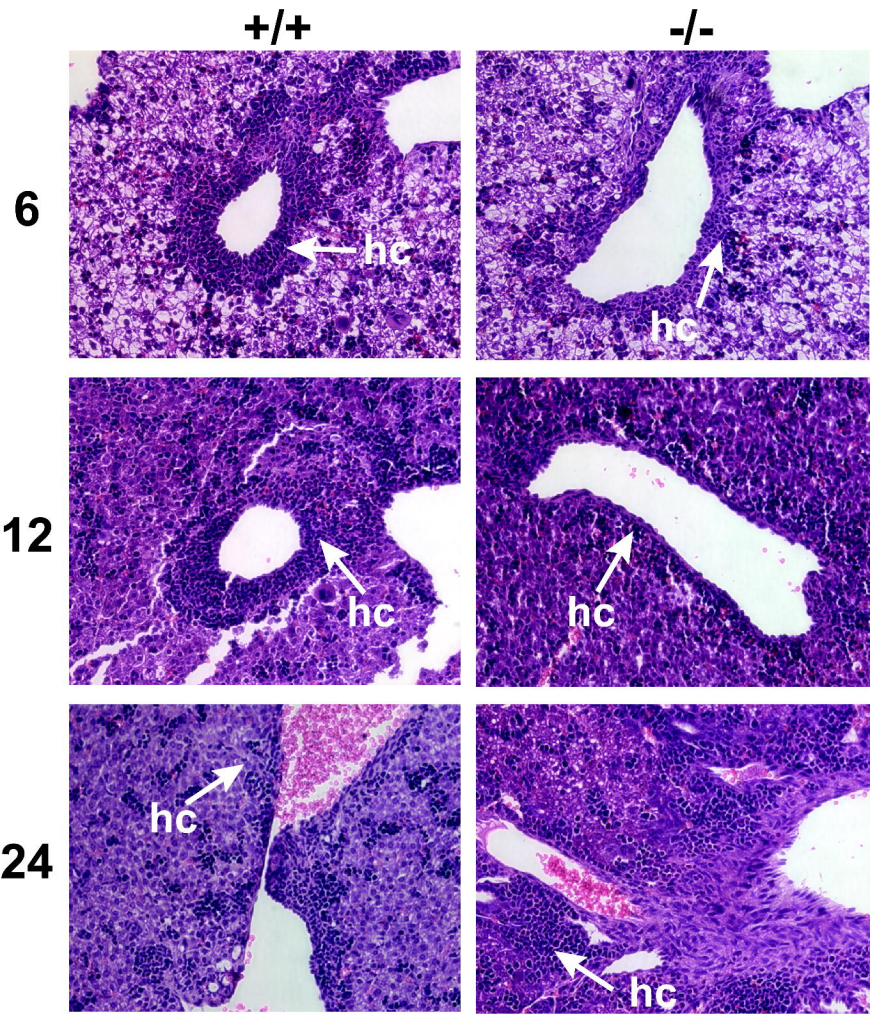

Figure 6.

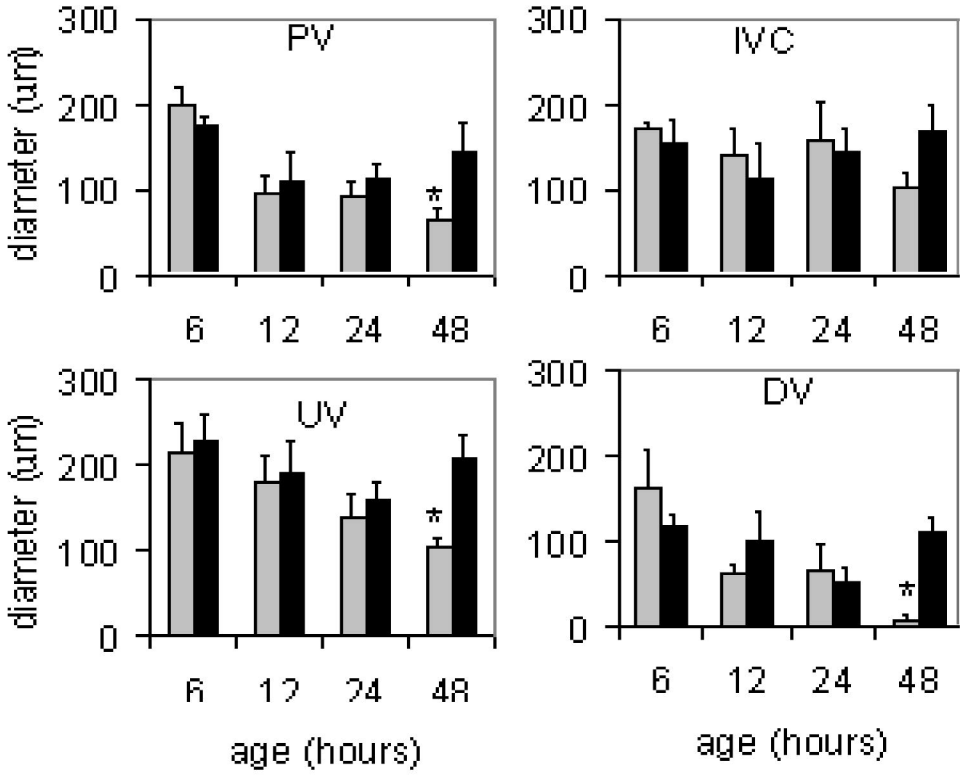

Figure 7.